9

OPTICALLY ANISOTROPIC METAL–POLYMER NANOCOMPOSITES

W. Caseri

Department of Materials, Institute of Polymers, ETH Zentrum, Zürich, Switzerland

1. INTRODUCTION

In composites based on polymer matrices with incorporated inorganic nanoparticles, a random dispersion of the particles is usually attempted. This is of particular importance with respect to the nanocomposites' optical properties. That is, if the particle sizes are far below the wavelength of visible light, scattering of visible light is strongly suppressed [1] and can typically be neglected in the resulting materials. This property renders nanocomposites attractive as materials with uncommon optical properties, which may be of use, for instance, in the area of photoconductivity [2, 3], nonlinear optics [2, 3], transparent magnetic materials [2, 3], transparent UV-absorbing layers [4–6], or extreme refractive indices [7–12]. However, nanocomposites with an ordered arrangement of nanoparticles have also been described, for example, in very thin films [13–19]. In fact, nanocomposites containing particles that form a regular lattice can show remarkable optical properties such as iridescence [20, 21]. In this chapter, however, anisotropic nanocomposites containing uniaxially oriented arrays of metal nanoparticles and their dichroic behavior are the main focus of our atten-

Metal-Polymer Nanocomposites, Edited by Luigi Nicolais and Gianfranco Carotenuto
ISBN 0-471-47131-3

tion. Dichroism, which is a phenomenon that has been studied for a long time in colored anisotropic crystals [22], can be recognized with simple methods: If a dichroic sample is placed before or behind a polarizer, the color of the sample changes upon rotation of the sample or of the polarizer. In ambient light, these colors are usually mixed and therefore not observed individually (unless the sample is in an appropriate position to naturally polarized light—for example, present in certain locations in the sky [23]). The color differences observed with polarized light emerge as a result of absorption differences of the two components of the light which are polarized perpendicular to each other.

The appearance of a color is a prerequisite for dichroism in the visible wavelength region, and this color can be introduced by metal nanoparticles. It is well established that metal nanoparticles are frequently colored, with the color depending on the type of metal and its particle size. For very small particles, the color is caused by absorption rather than by scattering, as demonstrated by Mie and Steubing about 100 years ago [24–27]. They found in the example of spheric gold particles with diameters below 50 nm that the intensity loss of transmitted light originated predominately from absorption [24–27]; considerable scattering arose only for gold particles with diameters above ~50 nm [28, 29]. In particle arrays such as present in the dichroic nanocomposites referred to below, it must be considered that the color of nanoparticles can depend not only on the size of the particles but also on the distance between the particles [30, 31]. This was realized about 100 years ago when Kirchner and Zsigmondy reported that nanocomposites of gelatin and colloidal silver [32] or gold [33] reversibly changed their color from blue to red upon swelling with water. They suggested that the color of nanocomposites must therefore be influenced by the distance between the embedded particles [32, 33], which was also substantiated around the same time by theoretical analyses of Maxwell Garnett [34, 35]. Hence, polarized light may interact with a particle array in a different way for parallel and perpendicular orientation of the polarization plane of the light with respect to the long axis of the particle array since cooperative optical effects that emerge in adjacent metal particles under the influence of electromagnetic radiation are more pronounced for parallel orientation (provided that the short axis of the particles is small enough).

2. DICHROISM IN NATURAL POLYMERS CONTAINING METAL NANOPARTICLES

Many fibers composed of natural polymers contain uniaxially oriented anisotropic hollow spaces in which metal particles can crystallize under appropriate conditions. As a consequence, the impregnated fibers contain anisotropic assemblies of metal nanoparticles that induce anisotropic optical properties

such as dichroism. In 1896, Ambronn prepared related materials. He immersed fibers or thin sections of natural polymers (leaches, cotton, and fir) for some time in the dark in an aqueous solution containing 1–2% silver nitrate [23]. Thereafter, he removed the specimen from the solution, let it dry in the air, and subsequently exposed it to ambient light for ~2 days whereupon the silver ions were reduced to elemental silver. Upon observation through a polarizer, the specimen appeared bright yellow or bright greenish for parallel orientation of the long axis of the fiber and the polarization plane of the light and appeared blue, green, red, or violet for perpendicular orientation. Dichroic samples could also be prepared upon *in situ* reduction of fine silver nitrate powder that had been strewed on dry plant fibers. This method was also successful for the preparation of dichroic animal sinews, white human hair, or gelatin that had been previously stretched (without stretching, dichroism in gelatin samples was not observed). Dichroic samples with stretched gelatin were also obtained after treatment with a silver-nitrate-saturated 80% ethanolic solution for several days. Moreover, upon immersion of natural fibers in aqueous or alcoholic solution of 1–2% gold chloride for some time followed by drying in the air and subsequent exposure to ambient light for 2–3 days, elemental gold was formed and a red color was found for parallel and blue-green or green for perpendicular orientation of the polarization plane of incident light and the long axis of the fiber. A related example prepared by Ambronn but displayed by Braun in 1905 [36] is shown in Figure 9.1. Reduction of the incorporated gold ions with formic acid was not successful for the manufacture of dichroic fibers, in contrast to the results mentioned below.

Only a short time after Ambronn's publication, Apáthy reported in 1897 that he had been busy for many years with the impregnation of animal fibers with gold salts that were subsequently converted to gold colloids by exposure to light (besides colloidal gold, Apáthy also considered the formation of AuO, according to a concept of the prominent chemist Berzelius) [37]. Apáthy studied the influence of a number of parameters on the reduction process and the quality of the coloration of the fibers. In the absence of light or organic matter, the characteristic colors that appear after reduction of gold salts to gold colloids were not observed, and the extent of the dichroism in the impregnated fibers depended on parameters such as the chemical composition ($H[AuCl_4] \cdot xH_2O$, where x was supposed to be 4, or $AuCl_3 \cdot xH_2O$, where x was supposed to be 0 or 2) and the commercial source of the gold salt, the amount of gold salt that was incorporated in the fiber, the temperature during the conversion into gold colloids, the presence of organic acids (formic acid, acetic acid, and citric acid), and the light intensity. The best results were obtained when the samples were immersed in a 1% $H[AuCl_4] \cdot xH_2O$ solution for 2 to ~12 hr in the dark followed by immersion of the wet samples into 1% formic acid. The reduction to gold colloids was then performed advantageously by subsequent exposure of the

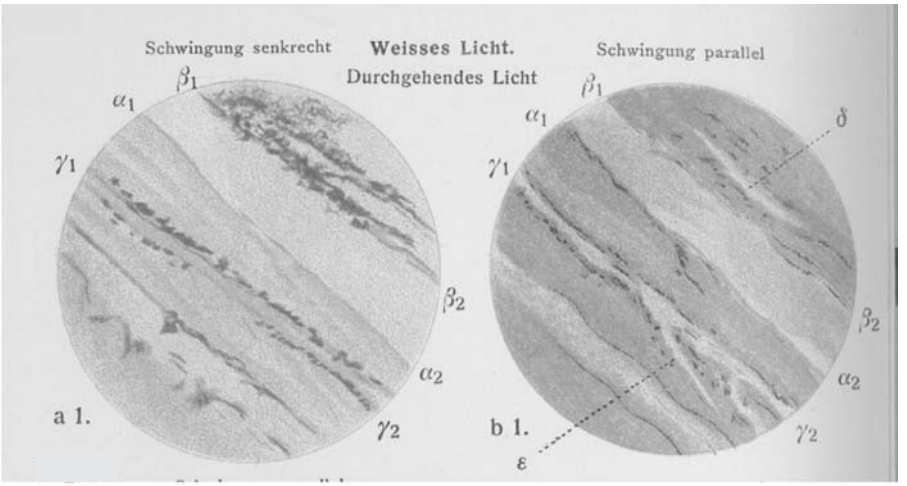

Figure 9.1. Microscope image of a dichroic nanocomposite consisting of gold particles embedded in wood (probably fir), published in 1905 [36]. The polarization plane of the light is parallel to the orientation axis of the wood in the left image and perpendicular in the right image. See color insert.

impregnated specimen to the light of a clear winter day during at least 8 hr without interruption at 10–15°C; however, at elevated temperatures in summer, exposure to diffuse daylight during at least 6 hr without interruption was recommended. The sizes of the formed gold particles were recognized to be below the resolution of an optical microscope, and the impregnated specimen adopted colors that varied from a bright pink to dark violet. Dichroism was observed at this type of specimen, with the colors changing for instance from cherry red at parallel orientation of the polarization plane to the long axis of the fibrils to blue-black at perpendicular orientation.

Dichroic samples in natural fibers had been prepared not only by reduction of metal salts in the fibers themselves. In the nineteenth century, dichroic specimen of gold or silver nanoparticles in gelatin were obtained by exposure of gelatin to dispersions of corresponding metal colloids followed by stretching of the swollen gelatin and subsequent drying [38]. A change in the position between the polarization plane of the incident light and the fiber direction from parallel to perpendicular orientation manifested in a color change in the case of gold from bright red or yellowish red to dark blue violet and in the case of silver from bright brown to dark brown or from yellow to olive green.

The elemental state of incorporated metal colloids in dichroic fibers was experimentally proven by early X-ray studies [39, 40]. The diffraction patterns

revealed that the crystal lattice of the silver and gold particles in ramie fibers did not differ from that of the the corresponding bulk metals [53, 60]. In the same era, a number of dichroic nanonomposites consisting of anisotropic natural polymers and gold [36, 39–48], silver [36, 39–41, 46–49], platinum [47], palladium [36, 47], rhodium [47], copper [47], bismuth [47], mercury [39, 44, 47, 48], or silver amalgam [48] were reported. The metal content in the fibers was determined only in relatively few cases. As an example, a silver content in cotton fibers of 0.02–0.2% w/w [46] and in ramie fibers of 0.1% and 5% w/w [46]—respectively 0.45% and 1.2% w/w (0.07% and 0.18% v/v) [49]—was found. In samples of gold in ramie fibers, metal contents between 0.6% and 1.6% w/w were measured [46]. For silver contents of as low as 0.1% w/w and gold contents of only 0.7% w/w, dichroism was weak but still just visible [46].

The dichroism in natural fibers with incorporated metal nanoparticles was found to depend strongly not only on the element employed [50] but also on the particle size [51], which was calculated from the full-width at half-maximum of X-ray diffraction patterns, yielding values between 5 and 14 nm in ramie, hemp, bamboo, silk, viscose silk, acetate rayon, and wool fibers [51]. As an example of a particle-size-dependent dichroism, a color transition between perpendicular and parallel orientation of polarization plane and long fiber axis in ramie fibers appeared from straw yellow to indigo blue for gold particles of 8.5-nm diameter and from claret red to green at 12.3-nm diameter [51].

It was suggested from the beginning that the dichroism in the nanocomposites composed of natural fibers and metal colloids must originate in an anisotropy in the context with the embedded metallic particles. Ambronn assumed the dichroism to be caused most likely by the formation of anisotropic, labile crystal modifications of the elemental metals [52], while Braun attributed the origin of the dichroism to metallic rods that are distributed in the matrix at appropriate distances for acting as a wire grid polarizer [36]. X-ray patterns of ramie fibers with incorporated gold particles showed well-formed rings stemming from the lattice of the metal atoms, demonstrating that the crystal axes of the metal particles were randomly oriented in the fibers, and it was concluded that the dichroism in those fibers was not due to an oriented anisotropic modification of silver or gold primary particles [40, 51] but was, instead, due to a uniaxially oriented linear arrangement of isotropic metal crystallites as a consequence of their growth in oriented, anisotropic spaces of the fibers (Figure 9.2) [50, 51, 53]. Hence, the particles themselves were considered not to be dichroic, and the dichroism was supposed to originate exclusively as a consequence of the anisotropic shape of the particle-filled space between oriented fibrils [50, 53]. It was also reported, however, that the X-ray diffraction patterns of silver in ramie fibers did not consist of completely homogeneous

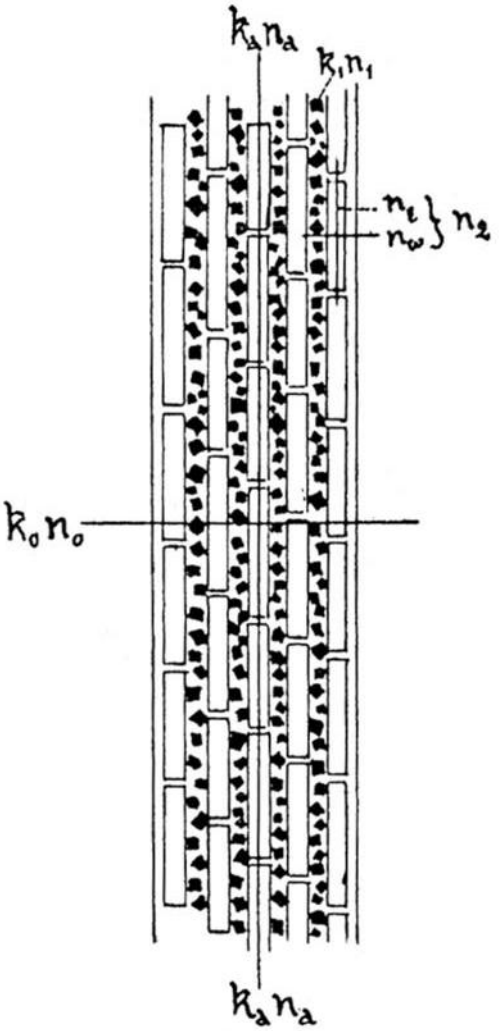

Figure 9.2. Schematic illustration of Frey's explanation of the dichroism in anisotropic natural fibers containing metal colloids, proposed in 1927 [50, 53].

rings but that they displayed some symmetric deviations [39], and it was therefore suggested that a fraction of the crystal axes of the metal particles was oriented, but another report considered these deviations in the X-ray diffraction patterns not to be significant [51]. Finally, observations in an ultramicroscope in combination with polarized light led to the conclusion that gold and silver particles in plant fibers (probably ramie) indeed were arranged in parallel elongated aggregates that caused the dichroic behavior of the samples [48].

3. DICHROIC FILMS OF POLY(VINYL ALCOHOL) AND GOLD NANOPARTICLES

For the preparation of dichroic nanocomposites based on poly(vinyl alcohol) (PVAL) as the matrix, colloids of elemental gold were synthesized *in situ* by reduction of sodium tetrachloroaurate(III) with trisodium citrate dihydrate in water [54, 55]. The colloidal gold dispersions thus obtained were added to aqueous PVAL solutions. The resulting homogeneous mixtures were poured in a flat dish; and after water evaporation, nanocomposite films were left. These films, which still contained reaction side products stemming from the reduction of tetrachloroaurate(III) with trisodium citrate, contained 3.4% w/w gold particles of 9.5-nm diameter. The incorporated gold particles were randomly dispersed in the PVAL, as evident from transmission electron microscopy (TEM), but agglomerates consisting of few particles might have been present, too. The absorption maximum in UV–Vis spectra, which appeared at 527 nm in aqueous dispersions of the gold particles, became broad in the isotropic nanocomposites and shifted to 564 nm (Figure 9.3).

The poly(vinyl alcohol)–gold nanocomposites were finally drawn at 120°C up to a draw ratio (DR), defined as the ratio of the length before and after drawing, of 5. It is well known that the polymer molecules orient upon drawing, and it was evident from TEM images of thin sections of the drawn materials

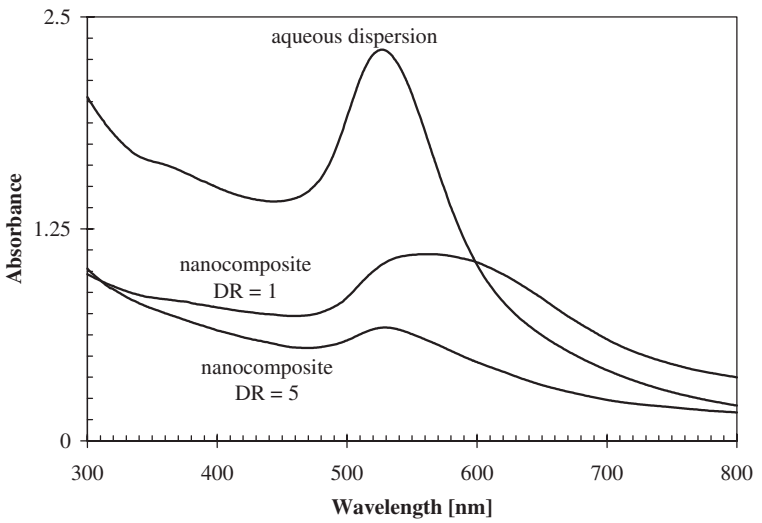

Figure 9.3. UV–Vis spectra of gold particles prepared *in situ* in water and of the related particles embedded in poly(vinyl alcohol) before drawing (DR = 1) and after drawing (DR = 5).

that the drawing also resulted in an alignment of a part of the gold particles into arrays that were oriented in the direction of the drawing axis. This alignment might arise as a consequence of the exclusion of particles between orienting polymer chains, thus maximizing the intermolecular forces between adjacent polymer molecules. The UV–Vis spectrum of the drawn samples recorded with nonpolarized light resembled to the spectrum of the gold colloids in aqueous dispersion (Figure 9.3; note that the absorbances in this figure have to be dealt with qualitatively since the amounts of particles in the optical path are not known), and the absorption maximum at 529 nm was close to that reported above in aqueous dispersion. This indicates that the size of the particles remained in the same order of magnitude upon preparation and processing of the composites as also evident from TEM images. The absorption maximum became sharper upon drawing, maybe as a consequence of a disruption or deformation of small particle agglomerates under the action of shear forces.

As in the case of the above-described natural fibers comprising metal nanoparticles, the color of the PVAL–gold nanocomposites changed upon observation in linearly polarized light as the angle φ between the polarization plane and the drawing axis was turned, as a consequence of the uniaxially oriented arrays of metal colloids. As an example, a specimen appeared blue for parallel ($\varphi = 0°$) and red for perpendicular ($\varphi = 90°$) orientation between the polarization plane of the incident light and the drawing axis. The color shifts of the nanocomposites upon variation of φ also manifested in UV–Vis spectra. The wavelength of maximum absorption (λ_{max}) shifted subsequently to shorter wavelengths as φ increased with λ_{max} at $\varphi = 0°$ at 528 nm and at $\varphi = 90°$ at 570 nm (Figure 9.4). Between 400 and 800 nm, the absorbance was higher at parallel than at perpendicular orientation of the polarization direction with respect to the drawing direction almost in the entire region, but between ~490 and 520 nm the absorbance was rather independent of φ.

4. DICHROIC FILMS OF POLY(ETHYLENE) AND GOLD OR SILVER NANOPARTICLES

Poly(ethylene) (PE) is a material that can be drawn to a higher extent than poly(vinyl alcohol) (the latter was the focus of Section 3). However, PE is insoluble in water; therefore, aqueous dispersions of *in situ*-prepared metal nanoparticles as described above are not suited for the preparation of PE–metal nanocomposites. Corresponding materials could be gained, however, by using precipitated metal nanoparticles surrounded by a layer of surface-bound organic molecules [54–59]. The organic surface layer prevented the formation of strongly connected agglomerates of metal particles in the isolated powder since the surface layer markedly diminishes the attractive interactions between metal

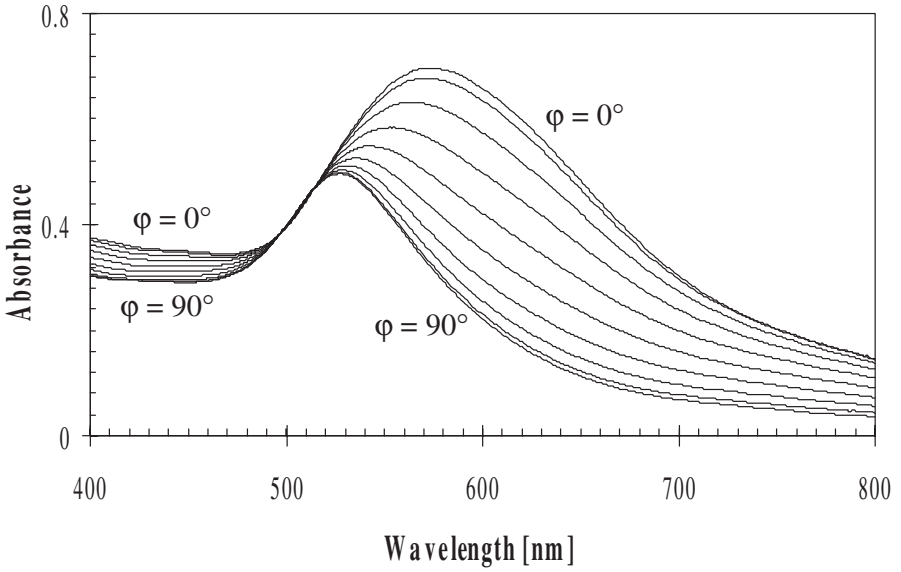

Figure 9.4. UV–Vis spectra of a drawn poly(vinyl alcohol)–gold nanocomposite in polarized light at different angles φ representing the angle between the polarization plane of the light and the drawing direction of the nanocomposite. The angle φ varies from 0° to 90° in steps of 10°, and a pure poly(vinyl alcohol) sample with similar thickness as the nanocomposite was inserted in the reference beam of the spectrometer.

particles; note that in absence of a surface layer the interactions between metal particles are so strong that the agglomerates usually cannot be disrupted during the processing steps for nanocomposite manufacture. For the creation of nanocomposites with PE, gold or silver particles coated with a layer of dodecanethiol were synthesized on the basis of previously described recipes [60, 61]. Gold or silver salts were reduced with sodium borohydride in a two-phase toluene–water mixture containing 1-dodecanethiol and tetraoctylammonium bromide as a phase transfer catalyst. Upon adsorption of the 1-dodecanethiol molecules on the *in situ*-formed metal particles, the metal colloids became well-soluble in toluene, and hence the organic phase adopted the color of the nanoparticles while the aqueous phase became completely colorless. Thereafter, the toluene phase was separated and the surface-modified colloids were precipitated by the addition of ethanol. Transmission electron microscopy (TEM) revealed average particle diameters of gold of 2–3 nm and of silver of 4–5 nm [54, 56, 57, 59].

Basically, surface-modified particles can be mixed with polymers present in the molten or in the dissolved state. However, when working with PE, it has

to be considered that some grades of PE are difficult to dissolve. A suited solvent for all PE grades is *p*-xylene at 130°C, and hence the dodecanethiol-coated particles were usually dispersed in *p*-xylene–PE solutions at 130°C followed by casting of the resulting mixture and solvent evaporation [54–59]. As an alternative route in the case of silver, the particles were also mixed with molten PE in an extruder at 180°C [57]. In order to improve the homogeneity of the nanocomposites, the solvent-casted and the extruded samples were compression-molded at 150–180°C; molding periods of 20 and 120 min resulted in materials with similar optical properties (cf. Table 9.1). The color of the surface-modified gold particles dispersed in *p*-xylene was retained in the nanocomposites prepared from the corresponding dispersions, and the absorption maxima (λ_{max}) in UV–Vis spectra of the *p*-xylene dispersions and the corresponding nanocomposites differed only slightly (0–20 nm, depending on the annealing period of the particles in xylene as described below), and the UV–Vis spectrum

TABLE 9.1. Absorption Maxima of Drawn Poly(ethylene)–Gold Nanocomposites (Draw Ratio 15) at Different Reaction Conditions and Different Angles φ Between the Polarization Plane of the Incident Linearly Polarized Light and the Drawing Axis of the Specimen[a]

C [% w/w]	t_h [min]	t_c [min]	$\lambda_{max}(0°)$ [nm]	$\lambda_{max}(45°)$ [nm]	$\lambda_{max}(90°)$ [nm]	$\Delta\lambda_{max}$ [nm]
3.75	90	20	542	534	527	15
		120	560	544	536	24
3.36	120	20	618	584	553	65
		120	619	575	548	71
3.75	180	20	614	570	546	68
		120	618	562	539	79
4.00	240	20	641	578	548	93
		120	648	571	541	107
3.96	300	20	690	580	534	156
		120	682	580	542	140
3.91	330	20	690	657	631	59
		120	678	640	618	60
4.18	480	120	676	641	614	62
3.85	810	20	653	625	607	46
		120	650	616	596	54

[a] Here c is the ratio of gold (including 1-dodecanethiol layer) and poly(ethylene), t_h is the heating period of the gold dispersion in a poly(ethylene) solution in *p*-xylene, and t_c is the compression molding period of the isotropic nanocomposites at 150°C. The absorption maxima at φ = 0°, 45°, and 90° are designated as $\lambda_{max}(0°)$, $\lambda_{max}(45°)$, and $\lambda_{max}(90°)$, respectively, and $\Delta\lambda_{max}$ is the difference between $\lambda_{max}(0°)$ and $\lambda_{max}(90°)$.

of the silver particles was essentially the same for the dispersion in *p*-xylene and the resulting PE–silver nanocomposites. However, in contrast to the initial gold dispersions in xylene and the resulting PE nanocomposites, aggregates of silver particles seemed to be present in the freshly prepared xylene dispersions and in the nanocomposites.

Sections of the nanocomposite sheets obtained after compression molding were drawn on a hot stage at 120°C up to maximum draw ratios of 22–60 depending on the grade of PE (high-density PE or ultrahigh-molecular-weight PE) [54–59]. Under appropriate conditions (which are described below), the drawing induced the formation of particle arrays which were oriented in the drawing direction (Figure 9.5), as evident from transmission electron microscope (TEM) and scanning electron microscope (SEM) images (an SEM picture displaying oriented arrays of gold particles is shown in Figure 9.6). The formation of oriented arrays of metal particles was connected with a dichroism in the resulting materials. Noteworthy, the extent of the dichroism of the drawn PE–gold nanocomposites strongly depended on an annealing period of the gold dispersions in the PE solutions used for nanocomposite preparation [54, 55, 59]. After drawing, most pronounced dichroism was observed when the gold particles had been kept in the PE–xylene dispersion at 130°C for 300–330 min before solvent evaporation (cf. Table 9.1). While the color of the mixture in xylene did not change significantly during heating for 1 hr, further annealing resulted in a color change from red to blue, and accordingly the absorption in UV–Vis spectra shifted to higher wavelengths (Figure 9.7). This effect might be due to an increase in the diameter of the primary gold particles [62, 63] or, as mentioned in the Introduction, to the formation of agglomerates. TEM images did not allow an unambiguous decision if the size of the primary gold particles changed during the treatment in *p*-xylene at 130°C. However, agglomerates were clearly evident in TEM images of samples that had been preannealed for 300 min [54, 59]. The cross section of these agglomerates ranged from a few up to ~10,000 primary particles. Agglomeration was not pronounced in TEM images without annealing of the gold dispersions in PE solutions in *p*-xylene or after annealing for 20 min. The agglomeration might be caused by partial desorption of the surface-bound dodecanethiol molecules, thus enhancing

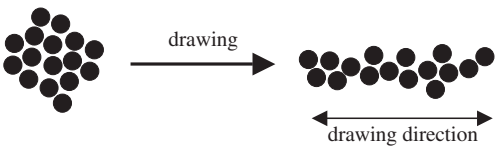

Figure 9.5. Schematic illustration of the deformation of spheric aggregates of metal particles into linear aggregates upon drawing.

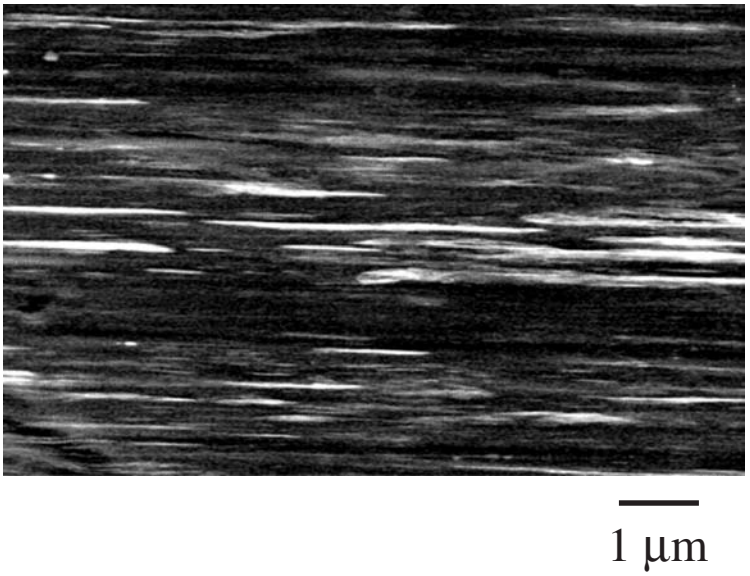

Figure 9.6. Scanning electron micrograph (detection of backscattered electrons) of a poly(ethylene)–gold nanocomposite. The bright lines represent arrays of gold nanoparticles that are not resolved individually.

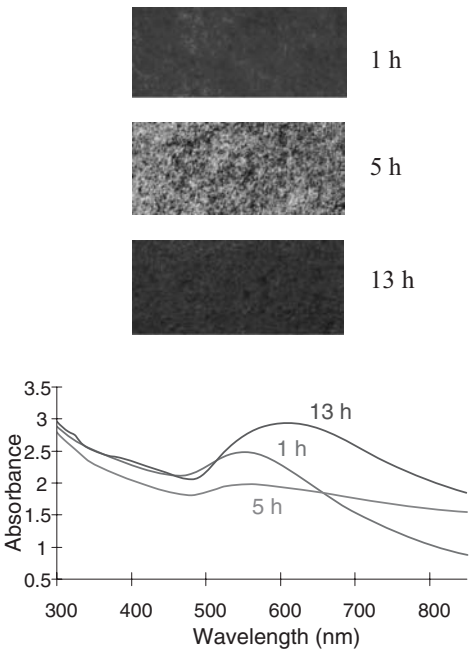

Figure 9.7. Colors and UV–Vis spectra of dispersions of gold particles (average diameter 2.2 nm, covered with a layer of 1-dodecanethiol) kept in a poly(ethylene) solution in *p*-xylene at 130°C for 1 hr, 5 hr, and 13 hr, respectively. See color insert.

the interactions between adjacent gold particles. Obviously, the aggregates of gold particles in the undrawn films were deformed during solid-state drawing of the nanocomposites, resulting in arrays of particles that were oriented in the drawing direction. Since the agglomeration of the gold particles required some time and thus the conditions became favorable for the formation of particle arrays only after a certain annealing period, only a weak dichroism was observed in drawn nanocomposites after annealing for 90 min—for example, with $\Delta\lambda_{max}$ (difference of the absorption maxima at $\varphi = 0°$ and $\varphi = 90°$) of ~15–25 nm compared to ~140–160 nm in nanocomposites prepared in the same way with the same grade of PE but with an annealing period of the gold dispersion in *p*-xylene of 300 min (Table 9.1). It has to be noted that dichroism also became less remarkable when the gold dispersion was kept in xylene at 130°C for periods significantly longer than 300 min—for example, with $\Delta\lambda_{max}$ of ~45–55 nm after 810 min annealing (Table 9.1)—probably as a result of an increase in the adhesion between the gold particles due to the desorption of a larger quantity of dodecanethiol molecules.

As already implied above, the UV–Vis spectra of drawn PE–gold nanocomposites gradually changed with φ in the UV and the visible wavelength range except at isosbestic points that emerged in all samples (an example of a UV–Vis spectrum is shown in Figure 9.8) [54, 55, 59]. The absorption maximum at parallel orientation of the polarization plane of the incident light ($\varphi = 0°$) appeared at higher wavelengths (typically between 670 and 690 nm, depending on the PE grade and the detailed experimental parameters) than at perpendicular orientation ($\varphi = 90°$, λ_{max} typically between 545 and 590 nm). Accordingly, the color of the drawn nanocomposites changed from blue at $\varphi = 0°$ to red at $\varphi = 90°$ (Figure 9.9).

Besides the annealing period of the gold particles dispersed in PE solutions in xylene, the influence of the amount of gold present in PE and the draw ratio

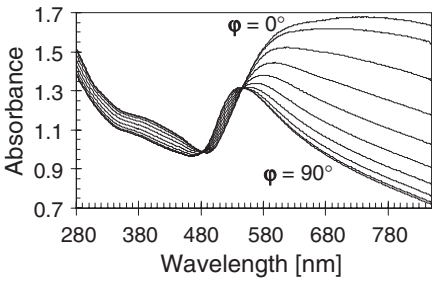

Figure 9.8. UV–Vis spectra of a drawn poly(ethylene)–gold nanocomposite in polarized light at different angles φ representing the angle between the polarization plane of the incident light and the drawing direction of the nanocomposite. The angle φ varies from 0° to 90° in steps of 10°.

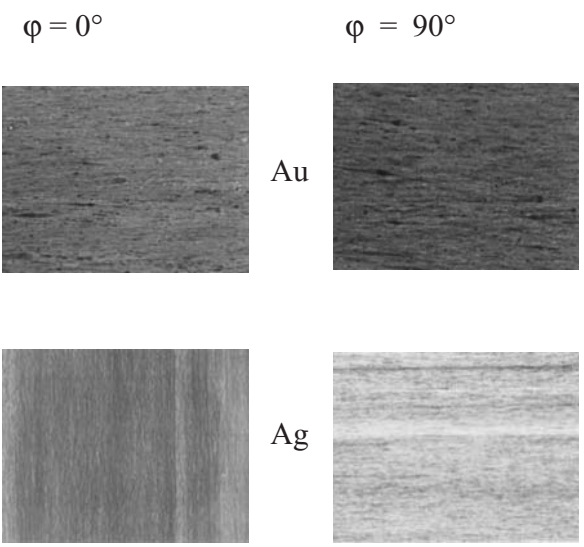

Figure 9.9. Colors of a drawn poly(ethylene)–gold and a poly(ethylene)–silver nanocomposite in polarized light with the polarization plane of the incident light and the drawing direction of the nanocomposite parallel (φ = 0°) and perpendicular (φ = 0°), respectively. See color insert.

on the dichroic properties of the composites was also investigated [54]. When the gold content was varied between 0.9% and 7.4% w/w, most pronounced shifts of the absorption maxima between φ = 0° and φ = 90° were observed in drawn samples with gold fractions of 2–4% w/w. The difference between the absorption maxima at φ = 0° and φ = 90° did not change exceedingly at draw ratios above 6. For example, a PE–gold specimen showed a $\Delta\lambda_{max}$ of 65 nm at a draw ratio of 6 and a $\Delta\lambda_{max}$ of 85 nm at a draw ratio of 18; and for oriented nanocomposites with another grade of PE, a $\Delta\lambda_{max}$ of 45 nm and 100 nm resulted for draw ratios of 10 and 45, respectively.

TEM micrographs of undrawn nanocomposites of PE and silver (Figure 9.10) revealed that the silver particles were agglomerated, to a certain extent, in the polymer matrix also without annealing of the silver dispersions in *p*-xylene containing dissolved PE, in contrast to the above-described behavior of the systems comprising gold particles. Aggregation of silver particles was also indicated by X-ray scattering patterns of undrawn nanocomposites that revealed lattice planes with a spacing of 3.5 nm [57]. As far as could be concluded from the individual silver nanoparticles that still were visible in TEM images of the nanocomposites, the size and size distribution of the primary particles did not change within the experimental precision upon preparation and processing of the nanocomposites. After drawing, an X-ray diffraction pattern with individ-

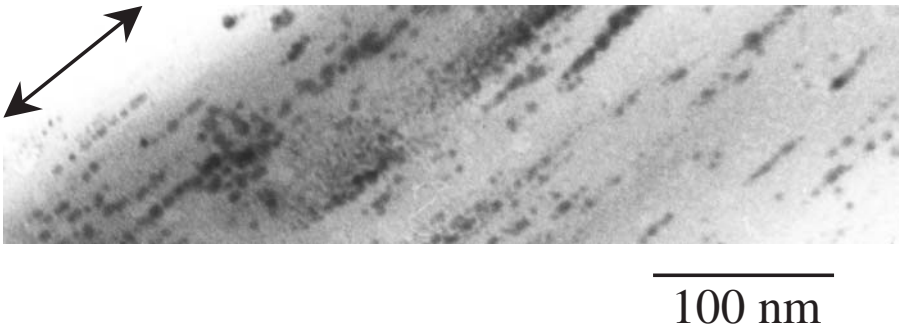

Figure 9.10. Transmission electron micrograph of a section of a drawn poly (ethylene)–silver nanocomposite showing uniaxially oriented arrays of silver particles. The doble arrow in the left upper corner indicates the drawing direction.

ual spots instead of rings was observed; the spots corresponded to lattice planes separated by 3.4 nm and indicated an orientation in the system. As described above for the gold particles, spheric aggregates formed by surface-modified silver particles in the undrawn materials also aligned into linear structures under the tensile deformation forces acting during solid-state drawing.

As in the case of the PE–gold nanocomposites described above, the UV–Vis spectra of the drawn PE–silver samples strongly depended on φ (an example is shown in Figure 9.11) [55–57]. Light with the polarization plane parallel to the drawing axis of the nanocomposites was absorbed at higher wavelengths than at the perpendicular orientation. As with drawn materials containing gold, isosbestic points also appeared in the UV–Vis spectra of drawn PE–silver nanocomposites. The PE–silver nanocomposites became dichroic at moderate draw ratios; in an example, $\Delta\lambda_{max}$ at $\varphi = 0°$ and $\varphi = 90°$ remained essentially constant (90 nm) between draw ratios of 6 and 22. The shift in the absorption maximum between $\varphi = 0°$ and $\varphi = 90°$ in the PE–silver samples was virtually independent of the procedure used for nanocomposite manufacture—that is, solution casting or melt processing. As implied by the UV–Vis spectra in polarized light at different φ, the color of the nanocomposites changed upon variation of φ, and the nanocomposites appeared red and yellow at φ of 0° and 90°, respectively (Figure 9.9). Annealing of PE–silver samples at 180°C for 15 hr resulted in an increase of the average particle size from 4.5 to 10 nm. The increase in particle diameter led to a shift of the absorption maximum in UV–Vis spectra from 435 nm to 463 nm. Accordingly, after drawing, the color turned from mauve or purple-red (depending on the sample) at $\varphi = 0°$ to amber at $\varphi = 90°$.

Dichroic nanocomposites with pronounced color changes are potentially useful in liquid crystal display (LCD) applications. The setup of a traditional

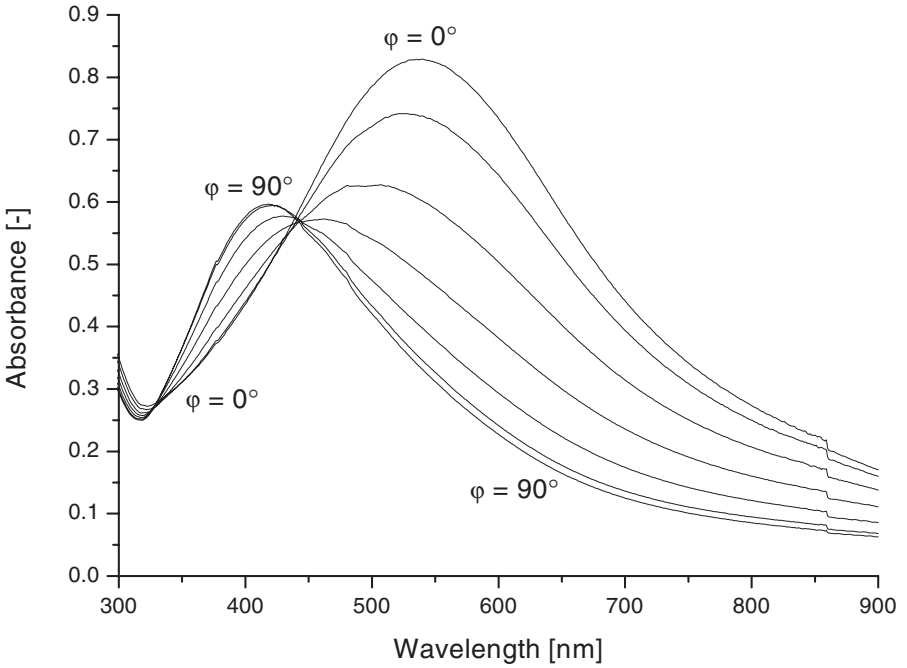

Figure 9.11. UV–Vis spectra of a drawn poly(ethylene)–silver nanocomposite in polarized light at different angles φ representing the angle between the polarization plane of the incident light and the drawing direction of the nanocomposite. The angle φ varies from 0° to 90° in steps of 15°.

LCD is shown in Figure 9.12. The incoming light passes two crossed polarizers that enclose an electrooptical cell containing liquid-crystalline molecules [64]. In the absence of a voltage, the liquid-crystalline molecules are arranged in a twisted-nematic structure that turns the direction of the polarization plane of the incoming light by 90°; that is, the light passes the second polarizer. In the presence of a voltage, however, the liquid-crystalline molecules orient parallel to the electric field and therefore the polarization plane of the incoming light does not change anymore; that is, this light is absorbed when arriving at the second polarizer. If, however, the second polarizer is replaced by a dichroic nanocomposite as described above with the drawing axis either parallel or perpendicular to the remaining polarizer, light is transmitted both in the absence and the presence of a voltage but in different colors (Figure 9.12), which results in a bicolored display [56, 59] instead of a common grayish/black display; an example is shown in Figure 9.13.

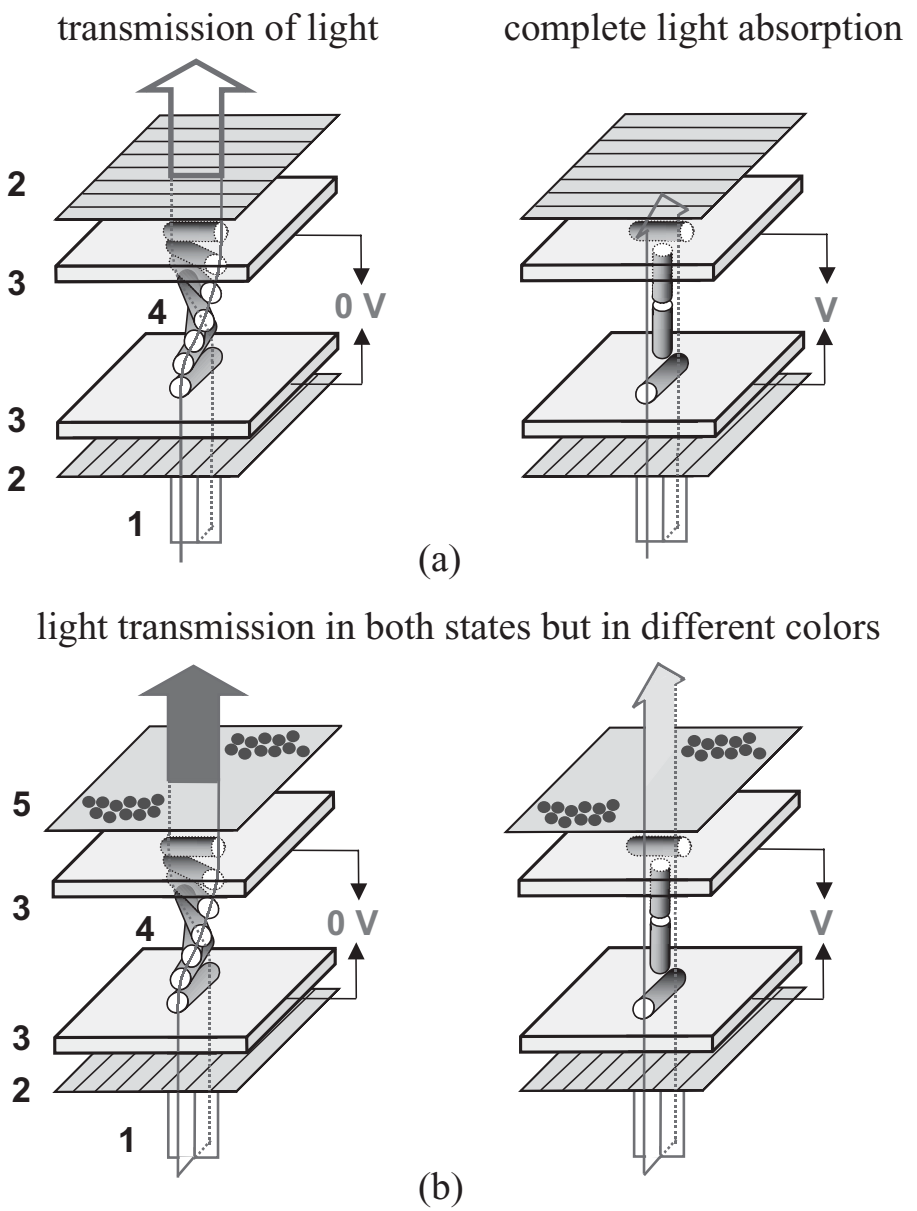

Figure 9.12. Schematic representation of **(a)** a standard twisted-nematic liquid crystal display and **(b)** a related display equipped with a drawn nanocomposite. 1, incoming light (unpolarized); 2, polarizer; 3, glass plate coated with an electrode layer and an orientation layer for the liquid-crystalline molecules; 4, liquid-crystalline molecules forming a 90° helical twist in absence of a voltage or a linear array parallel to an electric field in presence of an electric field; 5, nanocomposite with oriented arrays of metal particles. See color insert.

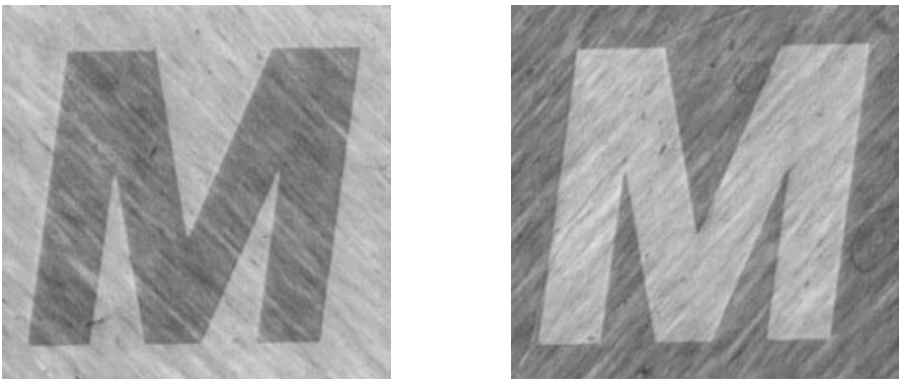

Figure 9.13. A twisted-nematic liquid crystal display (LCD) equipped with a poly(ethylene)–silver nanocomposite that had been annealed at 180°C for 15 hr and subsequently drawn as described in the text. The drawing axis of the nanocomposite is oriented parallel to the polarizer in the left image and perpendicular in the right image. See color insert.

6. CONCLUSIONS

Dichroic nanocomposites based on polymers with incorporated metal colloids can be prepared by *in situ* synthesis of the metal nanoparticles in fibers with oriented hollow spaces or by drawing of isotropic nanocomposites. In the former case, nanocomposites form uniaxially oriented aggregates in the originally present hollow spaces of the fibers; in the latter case, particle arrays oriented in the drawing direction are established as a result of the drawing process. In such composites, the absorption and hence the color of the samples observed in linearly polarized light depend on the angle φ between the polarization plane of the light and the orientation axis of the particle arrays. The resulting colors depend on the metal and the size of the primary particles and aggregates. The optical properties of such nanocomposites are similar to those of systems with wire-type metal entities [65–71]. Dichroic nanocomposites may find application, for example, in liquid crystal displays (LCD) that appear bicolored instead of grayish and black in corresponding standard displays.

ACKNOWLEDGMENTS

I express my thanks to my colleagues who have invaluably contributed to the results presented from our laboratory (including Figures 9.3 to 9.13), namely, Cees Bastiaansen, Cyril Darribère, Yvo Dirix, Wilbert Heffels, and Paul Smith.

REFERENCES

1. B. M. Novak, *Adv. Mater.* **5**, 422 (1993).
2. L. L. Beecroft and C. K. Ober, *Chem. Mater.* **9**, 1302 (1997).
3. D. Yu. Godovski, *Adv. Polym. Sci.* **119**, 81 (1995).
4. T. Kyprianidou-Leodidou, P. Margraf, W. Caseri, U. W. Suter, and P. Walther, *Polym. Adv. Technol.* **8**, 505 (1997).
5. R. J. Nussbaumer, W. R. Caseri, P. Smith, and T. Tervoort, *Macromol. Mater. Eng.* **288**, 44 (2003).
6. R. J. Nussbaumer, W. Caseri, T. Tervoort, and P. Smith, *J. Nanoparticle Res.* **4**, 319 (2002).
7. M. Weibel, W. Caseri, U. W. Suter, H. Kiess, and E. Wehrli, *Polym. Adv. Technol.* **2**, 75 (1991).
8. L. Zimmermann, M. Weibel, W. Caseri, U. W. Suter, and P. Walther, *Polym. Adv. Technol.* **4**, 1 (1993).
9. L. Zimmermann, M. Weibel, W. Caseri, and U. W. Suter, *J. Mater. Res.* **8**, 1742 (1993).
10. F. Papadimitrakopoulos, P. Wisniecki, and D. E. Bhagwagar, *Chem. Mater.* **9**, 2928 (1997).
11. T. Kyprianidou-Leodidou, W. Caseri, and U. W. Suter, *J. Phys. Chem.* **98**, 8992 (1994).
12. T. Kyprianidou-Leodidou, H.-J. Althaus, Y. Wyser, D. Vetter, M. Büchler, W. Caseri, and U. W. Suter, *J. Mater. Res.* **12**, 2198 (1997).
13. J. F. Ciebien, R. T. Clay, B. H. Sohn, and R. E. Cohen, *New J. Chem.*, 685 (1998).
14. V. Sankaran, C. C. Cummins, R. R. Schrock, R. E. Cohen, and R. J. Silbey, *J. Am. Chem. Soc.* **112**, 6858 (1990).
15. J. P. Spatz, A. Roescher, and M. Möller, *Adv. Mater.* **8**, 337 (1996).
16. M. Möller, J. P. Spatz, A. Roescher, S. Mössmer, S. T. Selvan, and H.-A. Klok, *Macromol. Symp.* **117**, 207 (1997).
17. S. T. Selvan, J. P. Spatz, H.-A. Klok, and M. Möller, *Adv. Mater.* **10**, 132 (1998).
18. J. P. Spatz, S. Mössmer, and M. Möller, *Chem. Eur. J.* **2**, 1552 (1996).
19. J. P. Spatz, S. Mössmer, M. Möller, T. Herzog, A. Plettl, and P. Ziemann, *J. Luminescence* **76&77**, 168 (1998).
20. H. B. Sunkara, J. M. Jethmalani, and W. T. Ford, *Chem. Mater.* **6**, 362 (1994).
21. J. M. Jethmalani and W. T. Ford, *Chem. Mater.* **8**, 2138 (1996).
22. H. Ambronn, *Anleitung zur Benutzung des Polarisationsmikroskops bei histologischen Untersuchungen*, J. H. Robolsky, Leipzig (1892).
23. H. Ambronn, *Kgl. Sächs. Ges. Wiss.* **8**, 613 (1896).
24. G. Mie, *Ber. Deutsch. Phys. Ges.* 492 (1907).
25. G. Mie, *Phys. Z.* **8**, 769 (1907).
26. G. Mie, *Z. Chem. Ind. Kolloide* **2**, 129 (1907).

27. W. Steubing, *Ann. Phys., vierte Folge (Drude's Ann.)* **26**, 329 (1908).
28. G. Mie, *Ann. Phys., vierte Folge (Drude's Ann.)* **25**, 377 (1908).
29. J. Turkevich, G. Garton, and P. C. Stevenson, *J. Colloid Sci. Suppl. 1* **9**, 26 (1954).
30. R. Zsigmondy, *Kolloidchemie, 1. Allgemeiner Teil*, Otto Spamer, Leipzig (1925).
31. M. Quinten and U. Kreibig, *Surf. Sci.* **172**, 557 (1986).
32. F. Kirchner, *Ber. Königl. Sächs. Ges. Wiss., Math.-Phys. Klasse* **54**, 261 (1902).
33. F. Kirchner and R. Zsigmondy, *Ann. Phys., vierte Folge (Drude's Ann.)* **15**, 573 (1904).
34. J. C. Maxwell Garnett, *Philos. Trans. R. Soc. London A* **205**, 237 (1906).
35. J. C. Maxwell Garnett, *Philos. Trans. R. Soc. London A* **203**, 385 (1904).
36. F. Braun, *Ann. Phys., vierte Folge (Drude's Ann.)* **16**, 238 (1905).
37. S. Apáthy, *Mitt. Zool. Stat. Neapel* **12**, 495 (1897).
38. H. Ambronn and R. Zsigmondy, *Ber. Sächs. Ges. Wiss.* **51,** 13 (1899).
39. F. Bion, *Helv. Phys. Acta* **1**, 165 (1928).
40. S. Berkman, J. Böhm, and H. Zocher, *Z. Phys. Chem.* **124**, 83 (1926).
41. H. Siedentopf, *Verh. Dtsch. Phys. Ges.* **12**, 6 (1910).
42. H. O. E. Patteri, *Z. Zellforsch. Mikrosk. Anat.* **16**, 723 (1932).
43. W. J. Schmidt, "Submikroskopischer Bau und Färbung des Chitins," in *3. Wanderversammlung Deutscher Entomologen in Giessen*, edited by F. van Emden and W. Horn, Dahlem, Berlin (1929), p. 100.
44. F. Fox, *Z. Farben-Textil-Ind.* **4**, 257 (1905).
45. W. J. Schmidt, *Z. Wiss. Mikrosk.* **52**, 8 (1935).
46. E. Kolbe, *Ueber die Färbung von Pflanzenfasern mit Silber- und Goldsalzen*, Ph.D. Thesis, Universitätsdruckrei von G. Neuenhahn, Jena, 1912.
47. A. Frey, *Z. Wiss. Mikrosk.* **42**, 421 (1925).
48. A. Frey-Wyssling, *Protoplasma* **27**, 563 (1937).
49. A. Frey-Wyssling and O. Wälchli, *J. Polym. Sci.* **1**, 266 (1946).
50. A. Frey, *Jahrbücher Wiss. Botanik* **67**, 597 (1927).
51. A. Frey-Wyssling, *Protoplasma* **27**, 372 (1937).
52. H. Ambronn, *Z. Wiss. Mikrosk.* **22**, 349 (1905).
53. A. Frey, *Das Wesen der Chlorzinkjodidreaktion und das Problem des Faserdichroismus (Ein Beitrag zur Theorie der Färbungen)*, ETH Habilitationsschrift, Zürich (1927).
54. W. Heffels, J. Friedrich, C. Darribère, J. Teisen, K. Interewicz, C. Bastiaansen, W. Caseri, and P. Smith, *Recent Res. Dev., Macromol. Res.* **2**, 143 (1997).
55. C. Bastiaansen, W. Caseri, C. Darribère, S. Dellsperger, W. Heffels, A. Montali, C. Sarwa, P. Smith, and C. Weder, *Chimia* **52**, 591 (1998).
56. Y. Dirix, C. Bastiaansen, W. Caseri, and P. Smith, *Adv. Mater.* **11**, 223 (1999).
57. Y. Dirix, C. Bastiaansen, W. Caseri, and P. Smith, *J. Mater. Sci.* **34**, 3859 (1999).

58. Y. Dirix, C. Bastiaansen, W. Caseri, and P. Smith, *Mater. Res. Soc. Symp. Proc.* **559**, 147 (1999).
59. Y. Dirix, C. Darribère, W. Heffels, C. Bastiaansen, W. Caseri, and P. Smith, *Appl. Optics* **38**, 6581 (1999).
60. J. R. Heath, C. M. Knobler, and D. V. Leff, *J. Phys. Chem. B* **101**, 187 (1997).
61. M. Brust, M. Walker, D. Bethell, D. J. Schiffrin, and R. Whyman, *J. Chem. Soc., Chem. Commun.* 801 (1994).
62. M. Ohtaki, Y. Ohshima, K. Eguchi, and H. Arai, *Chem. Lett.*, 2201 (1992).
63. C. A. Foss, G. L. Hornyak, J. A. Stockert, and C. R. Martin, *J. Phys. Chem.*, **98**, 2963 (1994).
64. M. Schadt and W. Helfrich, *Appl. Phys. Lett.* **18**, 127 (1971).
65. G. Chumanov., K. Sokolov, and T. M. Cotton, *J. Phys. Chem.*, **100**, 5166 (1996).
66. W. Gotschy, K. Vonmentz, A. Leitner, and F. R. Aussenegg, *Opt. Lett.*, **21**, 1099 (1996).
67. M. Takakuwa, K. Baba, and M. Miyagi, *Opt. Lett.*, **21**, 1195 (1996).
68. K. Baba, J. Katsu, and M. Miyagi, *Opt. Lett.*, **17**, 622 (1992).
69. K. Baba and M. Miyagi, *Opt Lett.*, **16**, 964 (1991).
70. A. H. Lu, G. H. Lu, A. M. Kessinger, and C. A. Foss, Jr., *J. Phys. Chem. B* **101**, 9139 (1997).
71. A. G. de León, Y. Dirix, Y. Staedler, K. Feldman, G. Hähner, W. R. Caseri, and P. Smith, *Appl. Opt.* **39**, 4847 (2000).